Design of cubic-phase optical elements using subwavelength microstructures

Mark S. Mirotznik[1], Joseph van der Gracht [2], David Pustai[3] and Scott Mathews[1]

[1]*Department of Electrical Engineering and Computer Science, The Catholic University of America, Washington, D.C. 20064*
[2] *HoloSpex, Inc. 6470 Freetown Rd., Ste 200-104, Columbia, MD 21044*
[3] *Lockheed Martin Corporation, P.O. Box 8048, Philadelphia, PA 19101*

Abstract: We describe a design methodology for synthesizing cubic-phase optical elements using two-dimensional subwavelength microstructures. We combined a numerical and experimental approach to demonstrate that by spatially varying the geometric properties of binary subwavelength gratings it is possible to produce a diffractive element with a cubic-phase profile. A test element was designed and fabricated for operation in the LWIR, ~ λ=10.6 μm. Experimental results verify the cubic-phase nature of the element.

OCIS codes: (050.6624) Subwavelength structures.

References

1. E.R. Dowski and W.T. Cathey, "Extended depth of field through wavefront coding," Appl. Opt. **34**, 1859-1866 (1995).
2. J. van der Gracht, E. R. Dowski, Jr., M. G. Taylor, and D. M. Deaver, "Broadband behavior of an optical-digital focus-invariant system," Opt. Lett. **21**, 919-920 (1996).
3. F. Xu, J. Ford, and Y. Fainman, "Polarization-selective computer-generated holograms: design, fabrication, and applications," Appl. Opt. **34**, 256-266 (1995).
4. M. S. Mirotznik, D. M. Pustai, D. W. Prather, and J. N. Mait, "Design of Two-Dimensional Polarization-Selective Diffractive Optical Elements with Form-Birefringent Microstructures," Appl. Opt. **43**, 5947-5954 (2004).
5. P. Lalanne and J. Hugonin, "High-order effective-medium theory of subwavelength gratings in classical mounting: application to volume holograms," J. Opt. Soc. Am. A **15**, 1843-1851 (1998).
6. E. Noponen and J. Turunen, "Eigenmode method for electromagnetic synthesis of diffractive elements with three-dimensional profiles," J. Opt. Soc. Am. A **11**, 2494-2502 (1994).
7. M. G. Moharam, D. A. Pommet, E. B. Grann, and T. K. Gaylord, "Stable implementation of the rigorous coupled-wave analysis for surface-relief gratings: enhanced transmittance matrix approach," J. Opt. Soc. Am. A **12**, 1077- (1995).
8. J. van der Gracht and G. Euliss, "Information optimized extended depth-of-field imaging systems," Proc. SPIE Aerosense Conf., Orlando, FL, (2001).
9. J. van der Gracht, P. Pauca, H. Setty, R. Narayanswamy, R. Plemmons, S. Prasad and T. Torgersen, "Iris Recognition with Enhanced Depth-of-Field Image Acquisition," Proc. SPIE Conference on Defense and Homeland Security, Orlando, FL, (2004).
10. J. van der Gracht, E. R. Dowski, W. T. Cathey, and J. Bowen, "Aspheric Optical Elements for Extended Depth of Field", SPIE Proceedings on Novel Optical System Design and Optimization, **2537**, San Diego, (1995).

1. Introduction

Dowski and Cathey proposed a new method of extending the depth of field of an imaging system involving the use of a suitable phase plate inserted into the pupil plane of a spatially incoherent imaging system [1]. While the encoded image is not visually pleasing, it can be digitally restored to produce a final image with improved depth-dependent detail. The term

#89957 - $15.00 USD Received 20 Nov 2007; revised 14 Jan 2008; accepted 15 Jan 2008; published 16 Jan 2008

wavefront coding describes the overall process of optical encoding at the pupil plane followed by digital restoration after detection. The first reported experimental demonstration of wavefront coding employed a modulo one wavelength element fabricated using a grayscale fabrication process [2, 10]. This fabrication process was borrowed from techniques used to generate diffractive elements. Subsequent reports of wavefront coded systems report the use of more conventional bulk optics fabrication techniques such as diamond turning.

In this letter, we report the use of a binary subwavelength diffractive element (DE) as an alternative to designing and fabricating a cubic-phase plate. One advantage of using subwavelength DEs is the ability to fabricate very thin and lightweight devices. In fact, the thickness of the subwavelength DE can be on the same order as the optical wavelength. Another possible advantage is the ability to generate polarization-dependent optical elements through the use of form-birefringence.

In [4] we described a design methodology for synthesizing polarization-dependent diffractive optical elements based on 2D form-birefringent gratings and a cell-encoding design algorithm. That technique yielded a single substrate binary element that generated nearly independent phase responses for horizontally and vertically polarized illumination. That method was demonstrated experimentally in the LWIR and was shown to be effective. To this end, we utilize the subwavelength cell-encoding procedure of [4] to design a polarization-insensitive cubic-phase plate. The phase plate was fabricated in silicon using electron-beam (e-beam) lithography and reactive-ion etching (RIE) and experimentally validated in the LWIR(10.6μm).

1.1. Design methodology general concept

Phase-only DEs are designed by mapping an electromagnetic wave's phase function into a surface relief pattern. Typically, the phase function is realized by modulating the height of an area whose dimensions are fixed for each phase value. This technique is referred to as point-oriented encoding. If the dimensions of the diffracting feature are much larger than the illuminating wavelength, the DE is designed using scalar diffraction theory. The degree of phase transformation is simply given as, $\nabla\phi = \frac{2\pi d}{\lambda_o}(n-1)$, where, d is the height of the dielectric feature, n is the index of refraction of the substrate, and λ_o is the free-space wavelength. However, if a periodic array of subwavelength features is used, then the degree of phase transformation is determined by the "effective" index of refraction of the subwavelength grating (i.e. $\nabla\phi = \frac{2\pi d}{\lambda_o}(n_{eff}-1)$). The effective index is a relatively sensitive function of the grating's period, feature shape, and thickness, as well as the bulk electromagnetic properties of the isotropic substrate. Thus, a large amount of freedom can be exploited in designing subwavelength DEs. Additionally, subwavelength gratings will respond anisotropically if either the grating periods (Λ_x and Λ_y) or feature shape differs along the *x*- and *y*-directions. This opens up the possibility of synthesizing polarization-dependent DEs [3, 4].

In [4] a design algorithm was presented that utilized a look-up table of the effective properties of subwavelength gratings as building blocks to synthesize more complicated DEs (illustrated in Fig. 1). The effective properties were pre-calculated using the rigorous coupled wave (RCW) method and used to generate more complicated spatially varying DEs. To insure that each grating generates only a zeroth diffractive order in both transmission and reflection, the grating periods, Λ_x and Λ_y, were restricted to less than λ_o, where λ_o is the free-space wavelength of illumination (i.e. subwavelength). For this paper, we utilized the cell-encoded algorithm to synthesize a cubic-phase optical element. In the next section, we briefly discuss our design procedure.

#89957 - $15.00 USD Received 20 Nov 2007; revised 14 Jan 2008; accepted 15 Jan 2008; published 16 Jan 2008

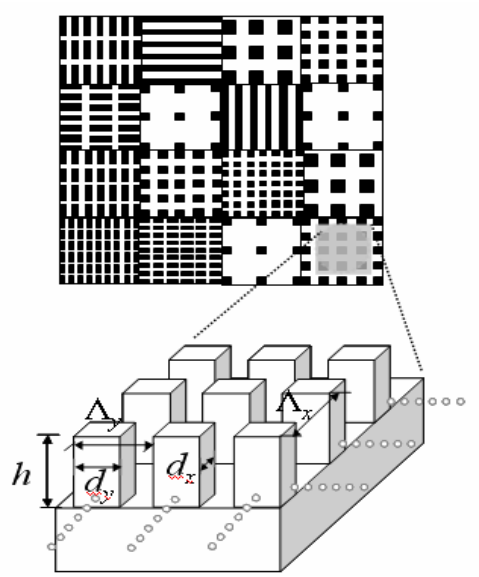

Fig. 1. Illustration of subwavelength cell-encoded element. At each cell of the DE a binary subwavelength grating is used to provide an effective property.

1.2. Effective properties of two-dimensional subwavelength gratings

Two approaches have been primarily used to determine the effective optical properties of subwavelength gratings. One uses closed form expressions [5] to provide approximate effective phase values as a function of the grating structure. Although attractive from a computational perspective, the approximate expressions are accurate only for gratings whose period is much smaller than the wavelength of illumination. As the grating period approaches the wavelength, which is referred to as the resonance regime, the closed form expressions become invalid.

We employ a second approach, which utilizes a rigorous electromagnetic model to determine the relationship between structural form and response. Although computationally more difficult, the approach is capable of generating accurate results for gratings of any period size and shape. Several rigorous electromagnetic models can be used for this calculation, however, our experience suggested that the RCW method offered the best compromise between accuracy and computational expense. To this end, we developed a rigorous model based on the method described by Noponen and Turunen [6] to calculate the effective electromagnetic properties of two-dimensional subwavelength gratings with rectangular features. For brevity, the mathematical details of the RCW method are not described here. For a detailed description the reader is referred to [6, 7].

1.3. Cell-encoded subwavelength diffractive elements

A cell-encoding scheme was employed to design DEs with spatially-varying effective properties. This process approximates a continuous phase response by a finite number of cells (as illustrated in Fig. 1). Each cell is assigned a single desired phase value. Given the look-up tables of effective properties, described in the previous section, it is relatively straightforward to identify a grating structure (i.e. grating periods and fill factors) at each cell that most closely matches the desired phase response at that location. It is important that the phase profiles are sampled on a scale larger than the wavelength. From trial and error we found that the phase profiles sampled as frequently as every five material wavelengths still produce good results. If the sampling distance is much smaller than this, the number of periods in the

#89957 - $15.00 USD Received 20 Nov 2007; revised 14 Jan 2008; accepted 15 Jan 2008; published 16 Jan 2008

subwavelength grating is insufficient to generate the predicted effective electromagnetic properties. However, if the sample distance is too large, the superwavelength phase profiles do not adequately represent the desired transformation. It should also be noted that by restricting the look-up tables to only those grating geometries that can by fabricated we have consequently integrated fabrication constraints into the design algorithm.

1.4. Design of a subwavelength cubic-phase element

Figure 2 illustrates the phase distribution of a cubic-phase optical element. Mathematically the complex transmittance of the cubic-phase element, P(x,y), is described by

$$P(x,y) = \exp(j\alpha[x^3 + y^3]/\lambda), |x| < \frac{L}{2}, |y| < \frac{L}{2}, \qquad (1)$$

where L is the width of the element and α determines the thickness of the phase element. A larger value of α leads to more depth invariance at the expense of detected images with poorer noise performance. If the value of α is chosen to be too small, the depth-invariant behavior is compromised. In this work, we initially chose a value of $\alpha = 14\pi$ intended to provide a reasonable balance between depth extension and noise performance. The choice of this value was guided by previous results based on information theoretic analyses [8] as well as prior successful experiments [9].

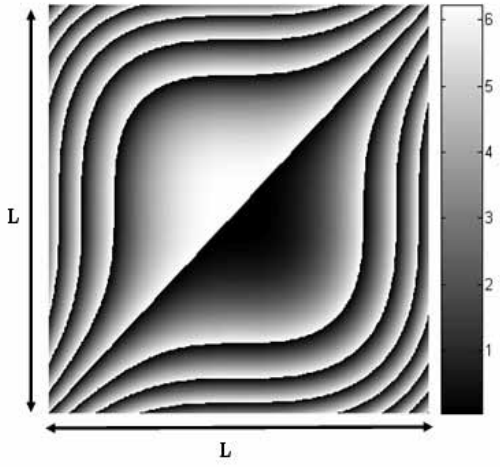

Fig. 2. Phase distribution of a cubic phase plate.

We design the element to be optimized for operation at a single wavelength, so the phase distribution $\phi(x,y)$ can be specified as follows,

$$\phi(x,y) = \mathrm{mod}\left[\frac{\alpha}{L^3}(x^3 + y^3), 2\pi\right], |x| < \frac{L}{2}, |y| < \frac{L}{2}, \qquad (2)$$

where L is the element size and the choice of $\alpha = 14\pi$ determines that seven 2π transitions will occur along the a slice taken through the x-axis. While the element is optimized for a single wavelength, useful broadband behavior has been demonstrated with a modulo one wavelength approach [2]. It is important to note that subwavelength diffractive elements are dominated by material dispersion which tends to exhibit better broadband behavior than diffractive dispersion.

#89957 - $15.00 USD Received 20 Nov 2007; revised 14 Jan 2008; accepted 15 Jan 2008; published 16 Jan 2008

Using the cell-encoding algorithm the continuous phase distribution shown in Fig. 2 is divided into a grid of N_x x N_y constant phase cells. At each cell location we assign a subwavelength grating whose effective properties most closely match the desired phase value at that cell location (illustrated in Fig. 3). Using this process we designed a subwavelength cubic-phase element in silicon for operation at 10.6 μm. The element size was 3mm x 3mm with a minimum subwavelength feature size of 500 nm and binary etch depth of 4.0 μm. The subwavelength features were pedestals with a square cross-section (as illustrated in Figs. 1 and 3). We also assumed the grating period in both the x and y dimensions, Λ_x and Λ_y, to be equal. By employing square pedestal features (i.e. equal fill factors in both the x and y dimensions) and equal period gratings (i.e. $\Lambda_x = \Lambda_y$) we ensure that the element's properties are isotropic. However, if we lifted this restriction an anisotropic cubic phase element could be designed so that it responded with completely independent phase variations depending on the state of polarization.

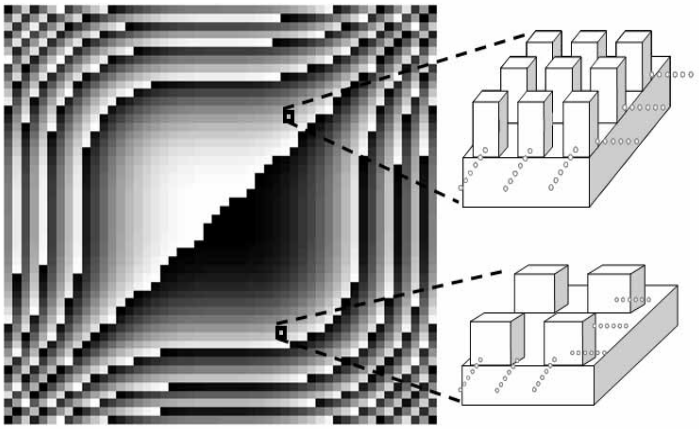

Fig. 3. Illustration of the subwavelength cell-encoding algorithm applied to a cubic phase element. The cubic phase distribution (shown in Figure 2) is decomposed into a finite number of cells. Each cell is formed by a suitable subwavelength grating.

2. Experimental fabrication and numerical simulations

To validate this method, we fabricated and tested the cubic-phase element described in the previous section as well as conducted numerical simulations. To fabricate the element, we first spun a 750 nm-thick layer of polymethyl methacrylate (PMMA) onto a double-sided polished silicon wafer and then patterned the PMMA using electron-beam lithography. After the PMMA was developed, silicon was etched using inductively-coupled plasma (ICP) reactive ion etching (RIE). Using a customized selective and anisotropic etch, we are capable of obtaining features as small as 50 nm with aspect ratios on the order of 10:1 and relatively flat sidewalls. In Fig. 4 the fabricated subwavelength cubic phase element is shown. The element was designed to have a binary etch depth of 4.4 μm which corresponds to a maximum phase delay of 2π radians at the 10.6 μm illumination wavelength. For the fabricated element we measured an etch depth of 4.0 μm. That error of 0.4 μm corresponds to a maximum phase error of 0.55 radians.

#89957 - $15.00 USD Received 20 Nov 2007; revised 14 Jan 2008; accepted 15 Jan 2008; published 16 Jan 2008

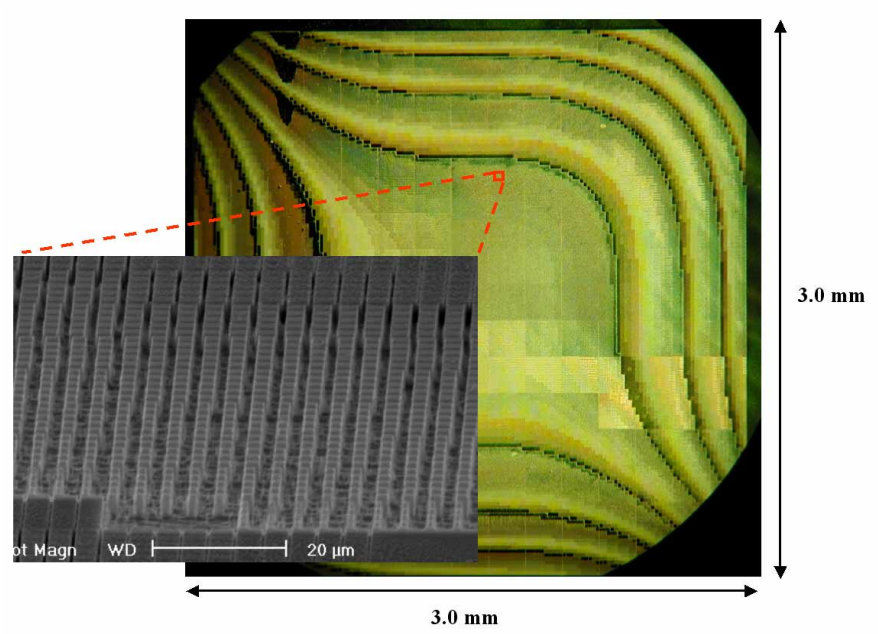

Fig. 4. Fabricated subwavelength cubic phase element. The insert shows a SEM image of the binary subwavelength gratings that make up the entire element.

The expected behavior of the cubic phase element can be modeled by appropriate simulation. We modeled the system as a linear-in-intensity imaging system, with a point spread function (PSF) given by the squared modulus of the Fourier transform of the complex amplitude transmittance of the effective phase at the pupil plane. In this work we use discrete Fourier transforms with appropriate zero padding to approximate a continuous Fourier transform. The focus invariance of the system can be seen by examining the behavior of the modulation transfer function (MTF) of the imaging system with varying amounts of quadratic phase error at the pupil plane. The MTF is given by the absolute value of the Fourier transform of the incoherent PSF. Once again, we employ discrete Fourier transforms with appropriate zero padding to approximate the Fourier transform.

Figure 5(a) shows the in-focus MTF taken along one of the axes and passing through the origin. The MTF slice was calculated for three different pupil plane phase functions corresponding to the ideal cubic phase profile (the blue line), the phase quantized design (the green line) and a phase quantized design that includes a phase error corresponding to an incorrect etch depth (the red line). The change in the MTF from the ideal to the phase quantized design shows only a modest difference. The modeled etch depth error, 0.4 µm, creates very little impact on the MTF behavior. This corresponds to the same etch depth error measured for the element described above.

Figure 5(b) shows the same MTF slices corresponding to the case of a strongly misfocused imaging system. The misfocus error is modeled by adding a quadratic phase term to the element pupil phase. The amount of phase error corresponds to one wavelength at the edge of the pupil aperture. Note that the overall behavior of the MTF does not differ greatly from the in-focus MTF slices. There is some slight reduction in magnitude at the higher frequencies. Also note that the phase errors created by the phase quantization and the etch depth error do not have significant effect on the MTF.

#89957 - $15.00 USD Received 20 Nov 2007; revised 14 Jan 2008; accepted 15 Jan 2008; published 16 Jan 2008

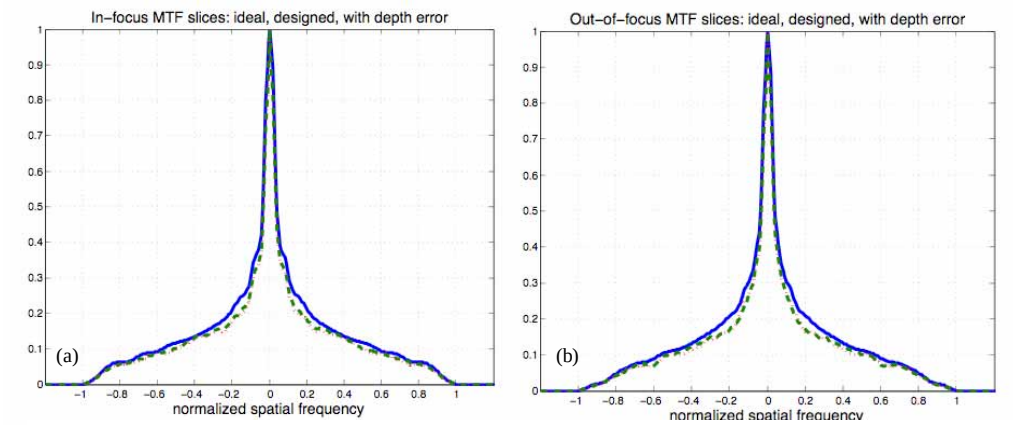

Fig. 5. MTF slices corresponding to the ideal cubic element (solid blue line), the phase quantized design (dotted red line) and the designed element with an added etch depth error (dashed green line). (a) Shows the MTF for the in-focus condition. (b) Shows the MTF for strong misfocus error of one wavelength.

The results of an end-to-end imaging simulation are shown in Fig. 6. The images were calculated using the linear-in-intensity model assuming an object comprised of a target at the in-focus position and an identically-shaped target at a depth position corresponding to one wave of misfocus aberration. The size of the target is assumed to be scaled such that the size of the two images at the image plane is identical. Figure 6(a) shows the image corresponding to a standard imaging system with no phase plate at the pupil plane. The blur is sufficient to obscure the finer features of the out-of-focus target. Fig. 6b shows the image of the same system after the subwavelength cubic element has been inserted. The model assumes both the phase quantization error and the etch depth error. While both targets appear significantly blurred, it is important to note that the nature of the blur appears to be quite similar for both targets.

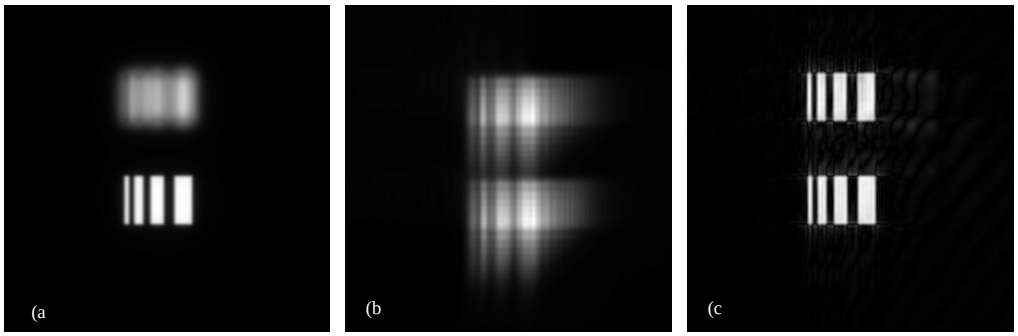

Fig. 6. Simulated images of two targets at different object distances. (a) The imaging system has a clear pupil aperture, (b) The imaging system model includes the designed cubic phase element modified by the measured fabrication etch depth error. (c) The image of (b) has been deblurred using a single Wiener restoration filter matched to the in-focus imaging condition.

A simple Wiener filter restoration was applied to the image in Fig. 6(b) to create the image in Fig. 6(c). The Wiener filter was computed using the incoherent PSF corresponding to the in-focus case. Since the filter is exactly matched to the in-focus imaging condition, the restored in-focus image is virtually identical to the ideal target image. More importantly, the same restoration produces a very high quality image of the out-of-focus target. Close

#89957 - $15.00 USD Received 20 Nov 2007; revised 14 Jan 2008; accepted 15 Jan 2008; published 16 Jan 2008

examination of the data does reveal some restoration errors, but the low magnitude of these errors provide an expectation that the subwavelength element can be used in conjunction with digital restoration to produce a highly focus-invariant imaging system. A real system would also have to contend with artifacts produced by system noise that can be troublesome when attempting to restore the higher frequencies in an image. These problems with noise and restoration are not unique to our subwavelength diffractive system. A careful digital restoration approach can be applied to strike a balance between high frequency feature restoration and noise performance.

3. Preliminary experimental results

We performed some preliminary experiments measuring the PSF of the fabricated element under a variety of mis-focus conditions. The expected PSF can be determined first with a simple simulation. First, consider imaging a distant compact point of light through an aberration-free imaging system having a clear circular pupil aperture. The Fourier transform of the clear circular aperture yields the expected Airy disc point spread function (PSF) at the image plane. For a cubic phase system, the PSF is estimated by computing the square magnitude of the Fourier transform of the expression for the cubic phase element while imposing the circular boundary produced by the aperture. Figure 7 shows the expected form of the resultant PSF as calculated using a Fast Fourier Transform (FFT) with appropriate zero-padding. The parameters were chosen to correspond to the designed phase excursion of the fabricated element. While the original design called for $\alpha = 7 * 2\pi$, over the 3 mm width of the element, the actual experiment required a 2.5 mm aperture to block unwanted light. This smaller effective size resulted in an effective value of $\alpha = 5.8 * 2\pi$. The shape and size of the PSF is highly invariant to misfocus [1]. Figure 7 also shows a simulated PSF corresponding to 1 wave of misfocus.

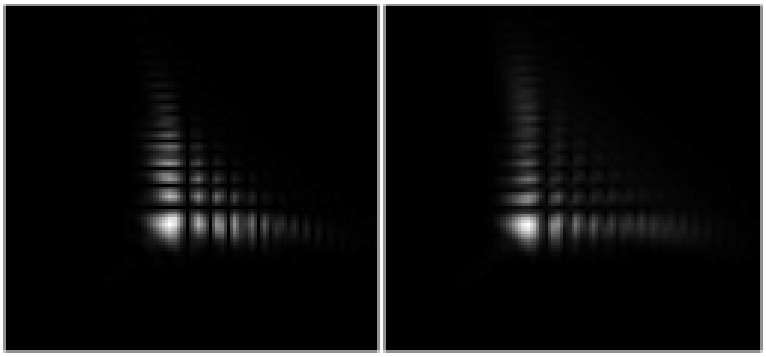

Fig. 7. Simulated PSF of a cubic phase element. The figure on the left predicts the PSF in the focal plane while the figure on the right predicts the PSF for 1 wave of misfocus.

We performed a simple proof-of-principle experiment to verify that the fabricated element produces the characteristic focus-invariant behavior of the cubic phase element. Figure 8 provides a schematic diagram of the experiment. A collimated tunable CO_2 laser beam, with a center wavelength of 10.6 μm, was focused onto a viewing screen with a 380 mm diameter infrared (IR) lens. Images on the viewing screen were digitally acquired using an IR camera and image grabber. In our experiment, the plane of best focus was 140 mm from the lens. The aperture containing the cubic element was placed in close proximity to the lens. We measured the response both with and without the cubic phase element in the aperture. For the case of no cubic element, we inserted an unetched double sided silicon wafer of similar thickness. Figure 8 shows that we additionally measured the response at planes far from best focus by moving the viewing screen.

#89957 - $15.00 USD Received 20 Nov 2007; revised 14 Jan 2008; accepted 15 Jan 2008; published 16 Jan 2008

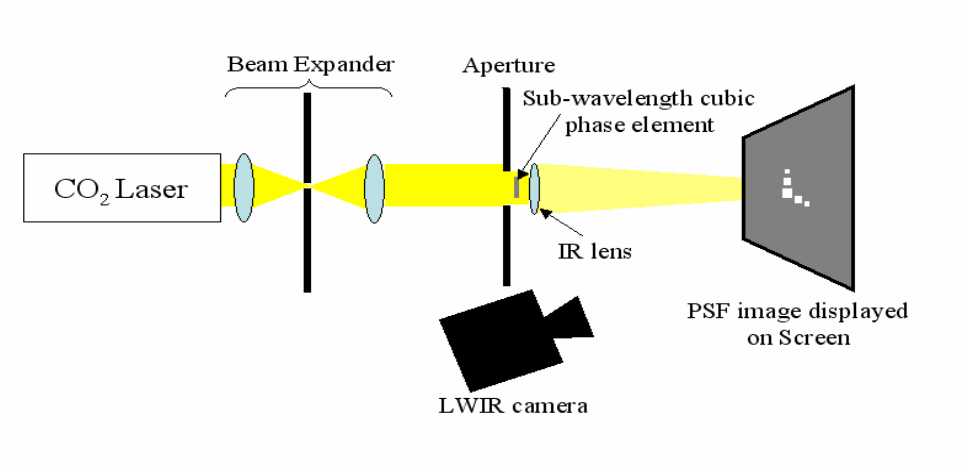

Fig. 8. Experimental setup used to characterize the subwavelength cubic element shown in Figure 4.

The detailed features of the measured response, shown in Fig. 9, differ from the predicted response, but the general behavior of the experimental PSFs follows that of the simulated PSFs. The overall shape of the laboratory-measured cubic phase element PSF has the characteristic "L-shape" as shown in the simulation of Fig. 7. It is important to note that the L-shape could not be produced by a binary phase element operating in the scalar wave regime since binary phase elements produce hermitian symmetric responses which would result in an additional duplicate response rotated by 180 degrees. Since our element was produced with binary depth etches, the non-symmetric PSF is explained by a vector electromagnetic model. Furthermore we note that the general shape and size of the cubic phase PSF remains relatively invariant over the focus range. In contrast, the traditional system PSF's vary as expected from a compact spot to a spot that significantly increases in width over the range of focus. Potential causes for the discrepancies between experiment and simulation include, (1) fabrication errors in the cubic element including a 0.4 μm etch depth error, (2) limitations in the dynamic range and resolution of the LWIR camera, (3) undiffracted light that generated a larger zeroth order spot than expected. Further study, however, is required to determine the exact reasons for the differences in the detailed features of the experimental and simulated PSFs.

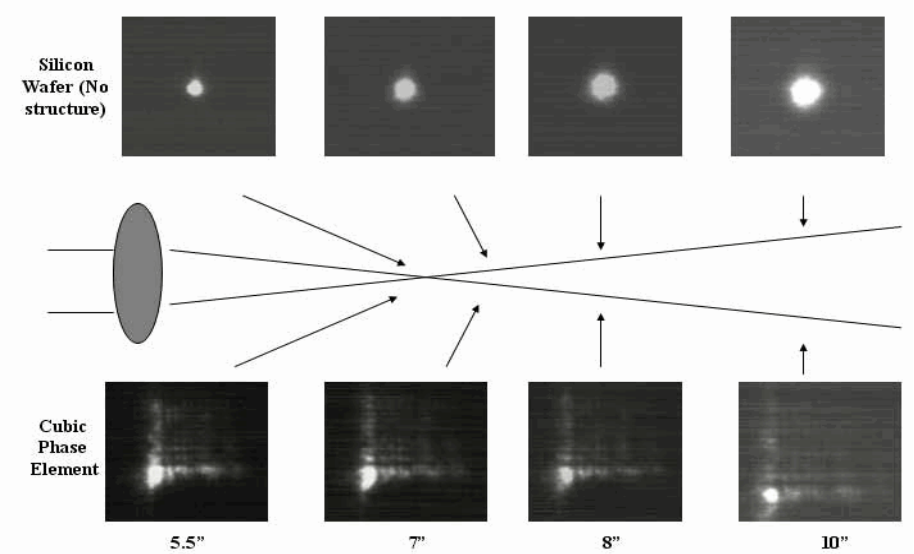

Fig. 9. Experimental results for the subwavelength cubic phase element reveal a PSF that exhibits the general behavior of a continuous phase cubic element and is reasonably invariant to misfocus.

#89957 - $15.00 USD Received 20 Nov 2007; revised 14 Jan 2008; accepted 15 Jan 2008; published 16 Jan 2008

4. Conclusion

Extended depth-of-focus imaging through pupil plane engineering has shown great promise in recent years. Many reported experiments employ a cubic-phase element to produce a focus invariant PSF that can be digitally restored during post-processing. Fabrication of the cubic phase elements, however, can be challenging problem. In this paper we described a design methodology for synthesizing cubic phase elements using subwavelength binary gratings. The method used a cell-encoding algorithm to produce very thin optical elements. A subwavelength cubic-element was fabricated for operation in the LWIR and characterized. The experimental results revealed the focus-invariant PSF properties of the cubic element. We are currently exploring the possibility of fabricating polarization dependent devices for applications in pupil plane engineering.

#89957 - $15.00 USD Received 20 Nov 2007; revised 14 Jan 2008; accepted 15 Jan 2008; published 16 Jan 2008